ACS APPLIED MATERIALS & INTERFACES

Research Article

www.acsami.org

Visualization by Neutron Diffraction of 2D Oxygen Diffusion in the $Sr_{0.7}Ho_{0.3}CoO_{3-\delta}$ Cathode for Solid-Oxide Fuel Cells

V. Cascos,*[,†] R. Martínez-Coronado,[‡] J. A. Alonso,[†] and M. T. Fernández-Díaz[§]

[†]Instituto de Ciencia de Materiales de Madrid, C.S.I.C., Cantoblanco, E-28049 Madrid, Spain

[‡]Texas Materials Institute and Materials Science and Engineering Program, The University of Texas at Austin, Austin, Texas 78712, United States

[§]Institut Laue Langevin, BP 156X, Grenoble F-38042, France

ABSTRACT: $Sr_{0.7}Ho_{0.3}CoO_{3-\delta}$ oxide has been recently described as an excellent cathode material (1274 mW cm^{-2} at 850 °C with pure H_2 as fuel[1]) for solid oxide fuel cells (SOFCs) with LSGM as electrolyte. In this work, we describe a detailed study of its crystal structure conducted to find out the correlation between the excellent performance as a cathode and the structural features. The tetragonal crystal structure (e.g., *I*4/*mmm*) basically contains layers of octahedrally coordinated $Co2O_6$ units alternated with layers of $Co1O_4$ tetrahedra sharing corners. An "in situ" neutron power diffraction (NPD) experiment, between 25 and 800 °C, reveals the presence of a high oxygen deficiency affecting O4 oxygen atoms, with large displacement factors that suggest a large lability and mobility. Difference Fourier maps allow the visualization at high temperatures of the 2D diffusion pathways within the tetrahedral layers, where O3 and O4 oxygens participate. The measured thermal expansion coefficient is 16.61 × 10^{-6} K^{-1} between 300 and 850 °C, exhibiting an excellent chemical compatibility with the electrolyte.

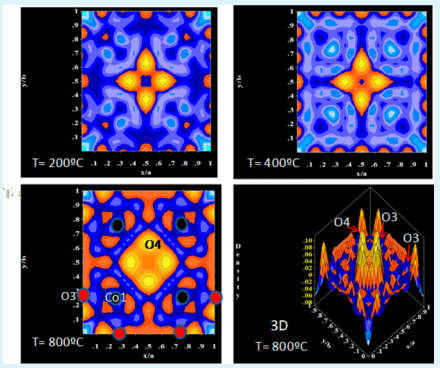

KEYWORDS: *cathode, IT-SOFC, $SrCoO_{3-\delta}$, $Sr_{0.7}Y_{0.3}CoO_{3-\delta}$, neutron diffraction*

1. INTRODUCTION

An intermediate-temperature solid oxide fuel cell (IT-SOFC) is an electrochemical device that converts chemical energy directly into electrical energy at temperatures between 550 and 850 °C; these devices have a high energy-conversion efficiency, low environmental impact, and good fuel flexibility.[2,3] The cathode is responsible for a significant drop in the cell potential at intermediate temperatures, thus one of the major improvements required for the commercialization of IT-SOFC is the development of new mixed ionic−electronic conductors (MIECs[4]) with better performance (lower resistance) at these temperatures.

Cobalt-based perovskite compounds have attracted a lot of attention as IT-SOFC electrodes due to their mixed-conducting characteristics and high ion conductivity in the intermediate temperature range.[5−7] Due to their properties, high-temperature $SrCoO_{3-\delta}$ phases with cubic 3C-like crystal structures (where the CoO_x coordination polyhedra share corners) are presented as mixed conductors with very high oxygen permeability.[8,9] At room temperature and normal pressure, $SrCoO_{3-\delta}$ oxide shows an approximate stoichiometry $Sr_2Co_2O_5$ that is able to adopt two very different structural types. When the samples are quenched from the reaction temperature (∼1000 °C) an orthorhombic brownmillerite-type structure is obtained (space group *Ima*2); in this metastable phase the oxygen vacancies are long-range ordered in layers of isolated CoO_4 tetrahedral zigzag chains, alternating with CoO_6 octahedral layers.[8,10] On the other hand, when the samples are slowly cooled from the reaction temperature, a hexagonal polymorph is obtained (space group *R*32).[11]

Whereas the brownmillerite-type structure displays excellent ionic and electronic transport properties, the hexagonal structure presents face-sharing CoO_6 octahedra, exhibiting almost non-oxygen permeability and poor electronic transport behavior. Unfortunately, orthorhombic brownmillerite irreversibly evolves to the unwanted hexagonal structure when heated above 650 °C; for this reason the stabilization of a 3C perovskite framework in the $SrCoO_{3-\delta}$ system has been a widely used strategy to obtain an adequate MIEC oxide in IT-SOFC. For this purpose, several substitutions have been performed by doping with several elements;[12−15] in a previous work[1,15] the 3C perovskite phase has been stabilized by doping at the Sr positions with different R^{3+} (R = rare-earth cations) yielding oxygen-deficient layered $Sr_{0.7}R_{0.3}CoO_{3-\delta}$ tetragonal oxides (space group *I*4/*mmm*). In particular, $Sr_{0.7}Ho_{0.3}CoO_{3-\delta}$ perovskite-related oxide[1] has been reported to exhibit an excellent performance as cathode material in IT-SOFC (1274 mW cm^{-2} at 850 °C with pure H_2 as fuel).

The aim of this work has been to carefully analyze the crystal structure of $Sr_{0.7}Ho_{0.3}CoO_{3-\delta}$ oxide to find out correlations with the excellent performance previously reported as cathode in SOFCs. For this purpose, a temperature-dependent neutron power diffraction (NPD) study has been undertaken. This

Received: March 4, 2014
Accepted: May 29, 2014
Published: May 29, 2014

   dx.doi.org/10.1021/am501297z | *ACS Appl. Mater. Interfaces* 2014, 6, 9194−9200

technique gave insight on the 2D diffusion paths of mobile oxygen atoms in the tetrahedral layers of the crystal structure under the working conditions of a SOFC. To complete the characterization, the thermal expansion and the chemical compatibility of this potential cathode material with the LSGM electrolyte have also been studied.

2. EXPERIMENTAL SECTION

$Sr_{0.7}Ho_{0.3}CoO_{3-\delta}$ polycrystalline powders were prepared by the citrate−nitrate route (soft-chemistry procedure). Stoichiometric amounts of analytical grade Ho_2O_3, $Sr(NO_3)_2$, and $Co(NO_3)_2{\cdot}6H_2O$ were dissolved under stirring in a citric acid aqueous solution containing some drops of HNO_3. The solution was slowly evaporated, leading to an organic resin that contains a homogeneous distribution of the involved cations. The formed resins were dried at 120 °C and decomposed at 600 °C for 12 h to eliminate the organic materials and the nitrates. The obtained precursor was then heated at 1100 °C for 12 h in air with an intermediate grinding. After the thermal treatment, the sample was quenched, thus leading to a pure tetragonal perovskite oxide phase.

The initial characterization of the product was performed by XRD with a Bruker-axs D8 Advanced diffractometer (40 kV, 30 mA), controlled by a DIFFRACT^{PLUS} software, in Bragg−Brentano reflection geometry with Cu K_α radiation (λ = 1.5418 Å) and a position sensitive detector (PSD). A filter of nickel allows the complete removal of Cu K_β radiation. For the structural refinement, NPD patterns were collected at the D2B diffractometer of the Institut Laue-Langevin, Grenoble, with a wavelength λ = 1.594 Å within the 2θ range from 10 to 153° at 25, 200, 400, and 800 °C. For the $T \geq 200$ °C collection, about 2 g of the sample was contained in a quartz tube open to the atmosphere and placed in the isothermal zone of a furnace with a vanadium resistor operating under vacuum ($P_{O2} \approx 1 \times 10^{-6}$ Torr). For the 25 °C measurement, about 2 g of sample was contained in a vanadium can; in all cases a time of 3 h was required to collect a full diffraction pattern. The NPD data were analyzed by the Rietveld method[16] with the FULLPROF program.[17] A pseudo-Voigt function was chosen to generate the line shape of the diffraction peaks. The irregular background coming from the quartz container was extrapolated from points devoid of reflections. In the final run, the following parameters were refined: scale factor, background points, zero shift, half-width, pseudo-Voigt corrected for asymmetry parameters, unit-cell parameters, positional coordinates, and isotropic displacement factors for all the atoms and anisotropic factors for O4 oxygen atoms at 800 °C. The coherent scattering lengths of Sr, Ho, Co, and O were 7.02, 8.44, 2.49, and 5.803 fm, respectively.

Measurements of the thermal expansion coefficient required the use of sintered cylindrical samples (5 mm diameter × 2 mm thickness). Densification was performed by uniaxial pressing of pellets that were subsequently calcined at 1100 °C for 12 h; the obtained density is around 90−95%. Thermal expansion of the sintered samples was carried out in a dilatometer Linseis L75HX1000, between 25 and 900 °C in air.

3. RESULTS AND DISCUSSION

3.1. Crystallographic Characterization. $Sr_{0.7}Ho_{0.3}CoO_3$ was obtained as pure, well-crystallized polycrystalline powders. The XRD diagram shown in Figure 1 is characteristic of a perovskite-type structure that can be indexed in a tetragonal unit cell with $a = b$ = 7.62263(4) Å and c = 15.3218(1) Å. The obtained unit-cell parameters are in excellent agreement with those reported in the literature ($a = b$ = 7.617 and c = 15.293 Å[1]). This cell is related to the cubic perovskite subcell parameter a_0 by $a \approx 2a_0$ and $c \approx 4a_0$. No impurity phases were detected.

To carry out a more exhaustive structural study of the $Sr_{0.7}Ho_{0.3}CoO_{3-\delta}$ perovskite, a neutron powder diffraction (NPD) study at room temperature and high temperature was performed. The crystal structure determined by NPD data at room temperature was defined in the $I4/mmm$ space group (No. 139), Z = 16. Two structural models were tested with our NPD data; in the former model[15,18−20] described for $Sr_{0.7}Y_{0.3}CoO_3$, Sr and Ho are distributed at random over three crystallographic sites, 4*e*, 8*g*, and 4*e*, with occupancy factors 0.7/0.3. In the second model, developed for $Sr_{0.7}Ho_{0.3}CoO_3$ from synchrotron XRD data,[21] a long-range ordering of part of Sr and Ho is proposed. Despite the rather similar Sr/Ho scattering lengths, we found that, indeed, Sr and Ho are partially long-range ordered. In our final model Sr1 and Ho1 atoms are ordered at two different 4*e* (0, 0, z) sites whereas (Sr,Ho)2 are distributed at random at 8*g* (0, 1/2, z). Two nonequivalent Co atoms are placed at 8*h* (x, x, 0) (Co1) and 8*f* (1/4,1/4,1/4) (Co2), and four oxygen atoms (O1, O2, O3, O4) are located at 16*n* (0, y, z), 16*m* (x, x, z), 8*i* (x, 0, 0), and 8*j* (x, 1/2, 0) Wyckoff positions, respectively. The occupancy factor for all the oxygens (O1, O2, O3, and O4) was also refined to determine the stoichiometric formula; O1 and O2 occupancies were fixed to unity since they converged to values close to 1. O3 converged to values slightly lower than 1, and O4 reveals an important number of vacancies (Table 1). The presence of these oxygen vacancies in the crystal structure is one of the factors that grants the excellent performance of this material as a cathode in SOFC. The final refined composition at 25 °C is $Sr_{0.7}Ho_{0.3}CoO_{2.70(1)}$. For the observed oxygen vacancies at room temperature, and assuming divalent and trivalent oxidation states for Sr and Ho, respectively, an average valence of $Co^{3.10+}$ is determined, indicating a mixed Co(III)−Co(IV) valence state at B-positions. Figure 2a illustrates the good agreement between the observed and calculated NPD patterns for this compound at room temperature. Table 1 contains the unit-cell parameters, atomic positions, occupancies, displacement factors, discrepancy factors, and selected interatomic distances after the Rietveld refinements of the crystal structure at room temperature.

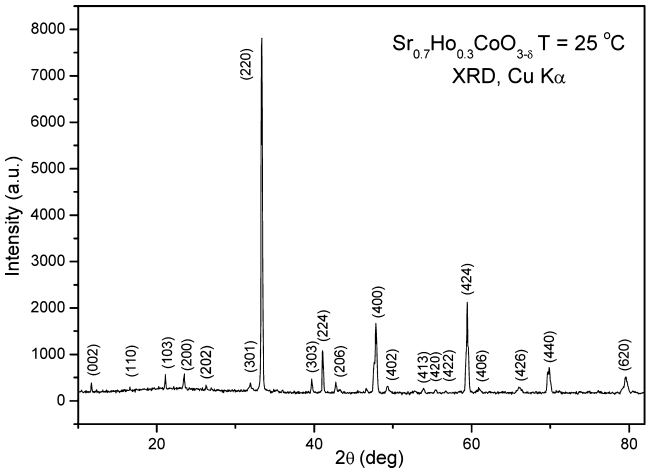

Figure 1. XRD pattern of $Sr_{0.7}Ho_{0.3}CoO_{3-\delta}$, indexed in a tetragonal unit cell with $a = b$ = 7.62263(4) Å and c = 15.3218(1) Å.

Figure 3 illustrates the crystal structure of $Sr_{0.7}Ho_{0.3}CoO_{3-\delta}$ that consists of CoO_6 octahedral layers containing Co2 atoms, which alternate with oxygen-deficient layers with Co1 atoms in CoO_4 tetrahedra; this layer consists of four CoO_4 tetrahedral groups, where each tetrahedra shares two oxygen atoms (O3) with the adjacent tetrahedra. Octahedral and tetrahedral layers share oxygen atoms (O2). Finally, extra oxygen atoms (O4) are situated in the tetrahedral layers, incrementing its coordination in fully disordered half-occupied positions.

In the octahedral layers, the CoO_6 groups exhibit an important axial distortion with four shorter equatorial distances Co2−O1 = 1.9111(2) Å and two longer axial distances Co2−O2 =

dx.doi.org/10.1021/am501297z | ACS Appl. Mater. Interfaces 2014, 6, 9194−9200

Table 1. Unit-Cell Parameters, Atomic Positions, Occupancies, Displacement Factors, Reliability Factors, and Selected Atomic Distances (Å) of $Sr_{0.7}Ho_{0.3}CoO_{3-\delta}$ in the Tetragonal *I*4/*mmm* (no. 139) Space Group, *Z* = 16, from NPD Data at 25, 200, 400, and 800°C

$Sr_{0.7}Ho_{0.3}CoO_{3-\delta}$	25	200	400	800
a (Å)	7.6196(1)	7.62963(9)	7.6538(1)	7.7110(1)
b (Å)	=	=	=	=
c (Å)	15.3174(4)	15.3791(2)	15.4366(3)	15.5650(4)
V (Å^3)	889.30(3)	895.24(2)	904.30(3)	925.48(4)
Sr1 4*e* (0, 0, *z*)				
z	0.8794(4)	0.8781(3)	0.8783(4)	0.8767(5)
B_{iso} (Å^2)	1.26(8)	1. 21(7)	1.76(9)	2.9(1)
f_{occ} Sr	1.00	1.00	1.00	1.00
Ho1 4*e* (0, 0, *z*)				
z	0.3517(2)	0.3515(2)	0.3522(2)	0.3525(3)
B_{iso} (Å^2)	0.75(7)	0.84(6)	1.03(6)	1.71(9)
f_{occ} Ho	1.00	1.00	1.00	1.00
(Sr,Ho)2 8*g* (0, 1/2, *z*)				
z	0.8680(2)	0.8686(2)	0.8686(2)	0.8690(3)
B_{iso} (Å^2)	0.81(5)	0.95(4)	1.36(5)	1.98(6)
f_{occ} (Sr/Ho)	0.90/0.10	0.90/0.10	0.90/0.10	0.90/0.10
Co1 8*h* (*x*, *x*, 0)				
x	0.7476(6)	0.7482(5)	0.7473(6)	0.7491(7)
B_{iso} (Å^2)	1.3(1)	1.26(9)	1.7(1)	2.3(1)
f_{occ} Co1	1.00	1.00	1.00	1.00
Co2 8*f* (1/4, 1/4, 1/4)				
B_{iso} (Å^2)	0.7(1)	0.59(7)	0.60(8)	1.77(1)
f_{occ} Co2	1.00	1.00	1.00	1.00
O1 16*n* (0, *y*, *z*)				
y	0.2452(3)	0.2450(2)	0.2446(3)	0.2466(4)
z	0.2402(1)	0.2397(1)	0.2402(1)	0.2401(2)
B_{iso} (Å^2)	0.87(3)	0.96(3)	1.29(4)	1.96(5)
f_{occ}	1.00	0.997(6)	1.00	0.991(6)
O2 16*m* (*x*, *x*, *z*)				
x	0.2859(2)	0.2858(2)	0.2864(2)	0.2872(2)
z	0.11758(2)	0.1175(1)	0.1170(2)	0.1165(2)
B_{iso} (Å^2)	1.79(5)	1.99(4)	2.48(5)	3.69(8)
f_{occ}	1.00	1.00	1.00	1.00
O3 8*i* (*x*, 0, 0)				
x	0.7200(6)	0.7188(5)	0.7210(5)	0.7162(8)
B_{iso} (Å^2)	1.7(1)	2.18(9)	2.5(1)	3.3(1)
f_{occ}	0.984(3)	1.00	1.00	1.00
O4 8*j* (*x*, 1/2, 0)				
x	0.383(1)	0.369(1)	0.370(1)	0.374(1)
B_{iso} (Å^2)	5.5(4)	6.8(4)	7.3(4)	8.7(6)
f_{occ}	0.412 (3)	0.422(7)	0.424(7)	0.446(8)
reliability factors				
χ^2	1.34	1.97	1.94	1.43
R_p (%)	2.23	1.46	1.41	1.23
R_{wp} (%)	2.83	1.86	1.84	1.55
R_{exp} (%)	2.44	1.32	1.32	1.30
R_{Bragg} (%)	3.92	4.21	4.85	3.34
distances (Å)				
Co1−O2 (*x*2)	1.836(1)	1.843(3)	1.843(3)	1.854(5)
Co1−O3 (*x*2)	1.935(5)	1.934(5)	1.945(5)	1.952(6)
Co1−O4 (*x*2)	2.133(8)	2.093(7)	2.094(8)	2.140(9)
Co2−O1 (*x*4)	1.9111(2)	1.914(2)	1.920(3)	1.934(4)
Co2−O2 (*x*2)	2.0649(4)	2.074(3)	2.091(3)	2.119(5)

2.0649(4) Å. This suggests the presence of intermediate spin Co^{3+} (*S* = 1) in Co2 sites, which would cause a Jahn−Teller elongation of the Co−O bond lengths, by shifting the O^{2-} ions from Co2 to Co1. In fact, the CoO_4 tetrahedra in the oxygen-deficient layers are compressed along the *c* axis with a much shorter Co1−O2 = 1.836(1) Å distance than the Co1−O3 = 1.935(5) Å bond lengths lying on the *ab* plane. Finally, Co1−O4 bond length is extremely long (2.133(8) Å) suggesting a much

dx.doi.org/10.1021/am501297z | ACS Appl. Mater. Interfaces 2014, 6, 9194−9200

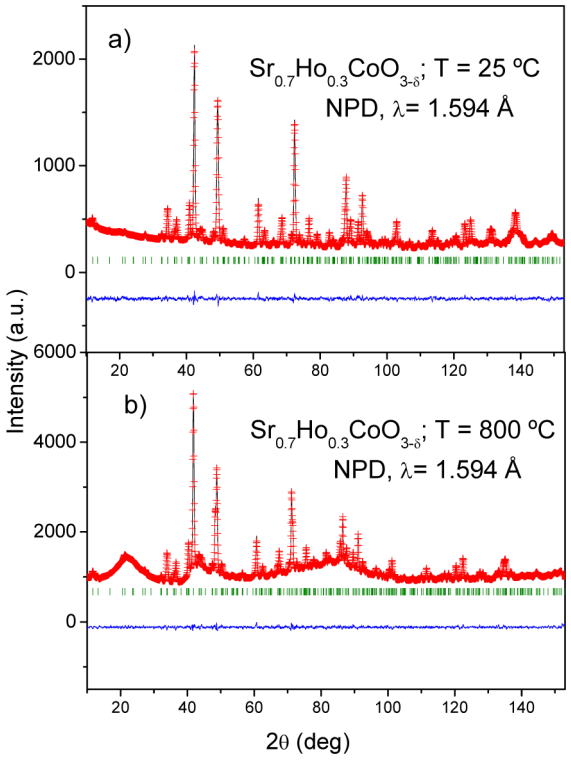

Figure 2. Observed (crosses), calculated (full line), and difference (at the bottom) NPD profiles for $Sr_{0.7}Ho_{0.3}CoO_{3-\delta}$ at 25 °C (a) and 800 °C (b) in vacuum (P_{O2} = 10^{-6} Torr), refined in the tetragonal *I*4/*mmm* space group. The vertical markers correspond to the allowed Bragg reflections. The irregular background observed in the high-temperature diagrams is due to the quartz container.

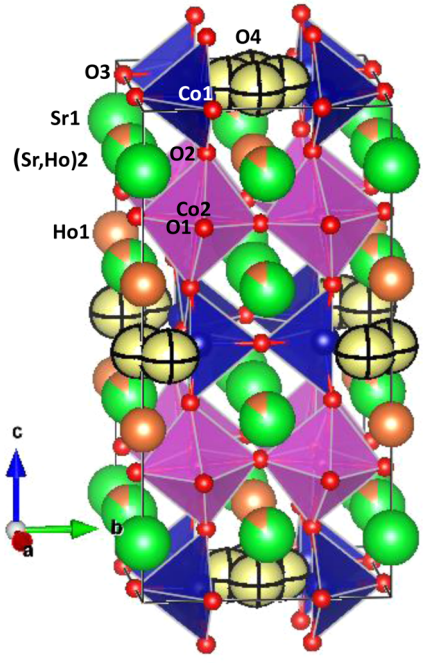

Figure 3. Crystal structure of the oxygen-deficient perovskite $Sr_{0.7}Ho_{0.3}CoO_{3-\delta}$. O1, O2, O3 atoms (red spheres), O4 (yellow spheres), Sr (green spheres), and Ho (pink spheres).

weaker bonding strength and therefore an extremely high lability for this oxygen atom. The unusually high thermal factor of 5.5(4) Å^2 for the O4 atoms at 25 °C also denotes that these oxygen atoms become mobile and disordered, showing a smeared scattering density. This diffusion is essential in mixed ionic and electronic conductors (MIECs), which is fundamental to obtain an excellent performance as a cathode.

The thermal evolution of the crystal structure under the cathode conditions in a SOFC was evaluated by NPD. The sample was contained in a quartz tube opened to the air atmosphere, and the NPD data were collected in situ at 200, 400, and 800 °C. The crystal structure is always defined in the *I*4/*mmm* space group, and no phase transitions to a higher symmetry were detected. Good agreement factors were obtained at the different temperatures for the perovskite structures. Figure 2b illustrates the excellent fit between the observed and calculated NPD patterns for this oxide at 800 °C. Table 1 includes the results obtained from the refinements at the different temperatures for $Sr_{0.7}Ho_{0.3}CoO_{3-\delta}$.

The thermal evolution of the oxygen content in air was also studied by NPD. Figure 4 illustrates the temperature dependence

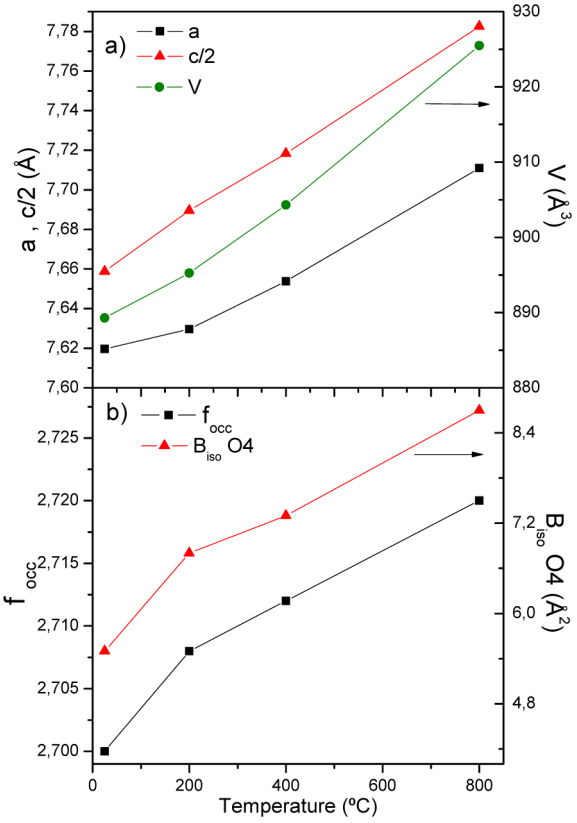

Figure 4. Thermal variation of (a) unit-cell parameter (left axis) and volume (right axis) and (b) oxygen occupancy factor (left axis) and isotropic displacement factors of the O4 oxygen (right axis), from in situ NPD data.

of the unit-cell parameters and the concentration of oxygen vacancies for $Sr_{0.7}Ho_{0.3}CoO_{3-\delta}$. As the sample is heated, the volume of the cell increases from 889.30 Å^3 at 25 °C to 925.48 Å^3 at 800 °C (Figure 4a), due to the expected thermal expansion. The oxygen content barely varies from $Sr_{0.7}Ho_{0.3}CoO_{2.70(1)}$ at 25 °C to $Sr_{0.7}Ho_{0.3}CoO_{2.72(1)}$ at 800 °C (Figure 4b); the abundant oxygen vacancies observed at high temperature are essential to drive the required O^{2-} motion in a MIEC oxide. Finally, the isotropic displacement factors (B_{iso}) of the O4 oxygen atoms exhibit a significant increase as the temperature rises (Figure 4b),

dx.doi.org/10.1021/am501297z | ACS Appl. Mater. Interfaces 2014, 6, 9194−9200

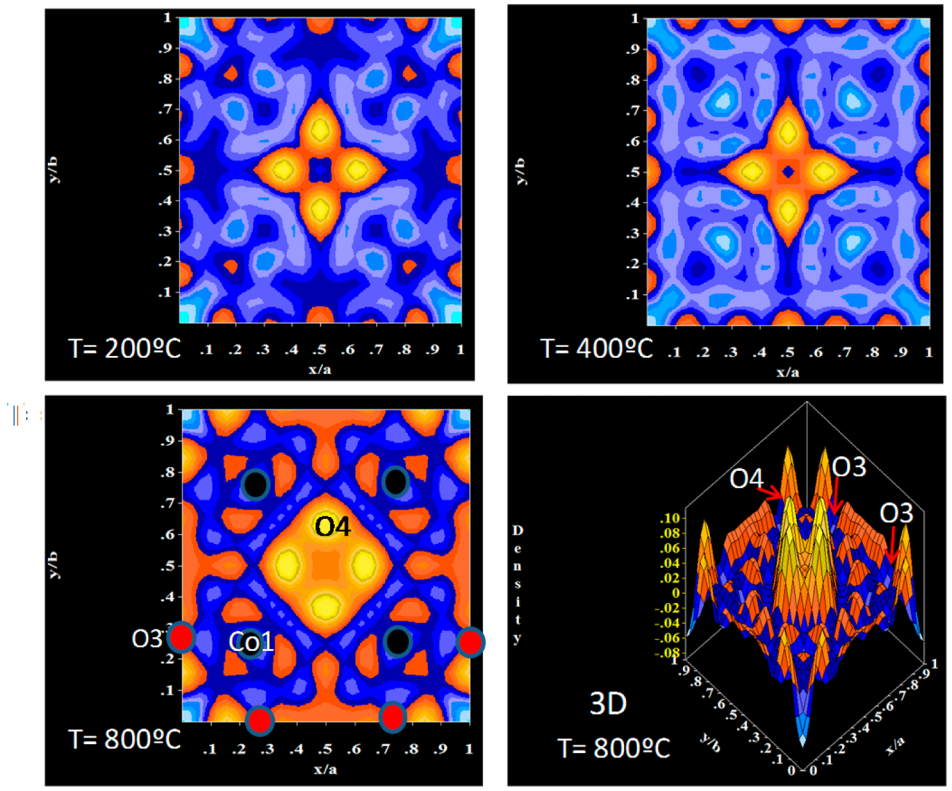

Figure 5. Difference Fourier maps at 200, 400, and 800 °C for $z = 0$ in a model where O4 atoms have been removed. O4 peaks are clearly located at 8*j* sites; as *T* increases the intermediate nuclear density indicates that O is delocalized on the ac plane. The right lower 3D graph shows intermediate density between the O3 nominal positions.

taking values as high as 8.7(6) Å^2 at 800 °C, which again reveals a high mobility or chemical lability of these oxygen atoms, suggesting a high ionic conductivity at the working temperatures of the SOFC.

An interesting insight onto the O^{2-} motion was achieved by removing O4 atoms from the structural model and performing difference Fourier syntheses from observed and calculated NPD data at increasing temperatures. The difference between observed and calculated structure factors contains information on the missing scattering density (in this case nuclear density) and its possible smearing in the real space. Figure 5 shows the evolution of the difference Fourier maps corresponding to the $z = 0$ section for T = 200, 400, and 800 °C, where strong positive peaks corresponding to the 8*j* (0.38, 1/2, 0) sites for O4 are observed in the center of the diagrams, and some intermediate nuclear density progressively appears at 8*j* (0.18, 1/2, 0) sites, between O4 peaks and those of the contiguous cells, indicating that O becomes partially delocalized as temperature increases. At 800 °C the 3D plot (right lower panel) also shows a significant positive scattering density between the nominal positions of the O3 oxygen atoms, indicating that O3 also participates in the ionic conduction process at such high temperatures. Also it is interesting to note that an anisotropic refinement of the O4 positions, affected by a huge displacement factor at 800 °C of ≈9 Å^2, yields very similar ellipsoid semiaxes suggesting a rather isotropic vibration for O4, as represented in Figure 3. This may be related to the weak character of the chemical bonds to Co, in agreement with the lability and free mobility exhibited by these oxygen atoms, in close connection with the excellent MIEC properties of this perovskite as cathode material in SOFC.

3.2. Chemical Compatibility and Thermal Expansion Measurements. Aiming to determine the mechanical compatibility of the $Sr_{0.7}Ho_{0.3}CoO_{3-\delta}$ oxide with the other SOFC components, thermal expansion measurements were performed in an oxidizing atmosphere. The thermal expansion was measured on dense cylindrical pellets (5 mm diameter × 2 mm thickness) sintered at 1100 °C for 12 h in air. The dilatometric analysis was carried out between 25 and 900 °C for several cycles in air; the data were only recorded during the heating runs. Figure 6 shows no abrupt changes in the thermal expansion in all the temperature ranges under measurement. TEC measured under air atmosphere between 400 and 850 °C is 16.61 × 10^{-6} K^{-1}, which is in good agreement with that calculated in the same temperature range by NPD data (15.15 × 10^{-6} K^{-1}). Although the thermal expansion coefficient obtained for $Sr_{0.7}Ho_{0.3}CoO_{3-\delta}$ is considerably higher than those of the typical electrolytes, which are between 10 and 13 × 10^{-6} K^{-1}, it is much lower than those presented by other Co perovskite materials[22,23] that have been successfully used as electrode materials.

Finally, the chemical compatibility between $Sr_{0.7}Ho_{0.3}CoO_{3-\delta}$ and the electrolyte (LSGM) was studied by grinding both materials in equal amounts and heating at 1100 °C for 24 h in air atmosphere. The inset of Figure 6 shows the refined XRD diagram of the calcined mixture, which does not reveal any chemical reaction between the oxide and the electrolyte, avoiding the formation of unwanted secondary phases when the material is tested in single cells.

By different experimental techniques we have tried to give an interpretation of the good behavior of this perovskite as a cathode in SOFC. The close inspection of subtle structural details together with the macroscopic properties concerning the

dx.doi.org/10.1021/am501297z | ACS Appl. Mater. Interfaces 2014, 6, 9194−9200

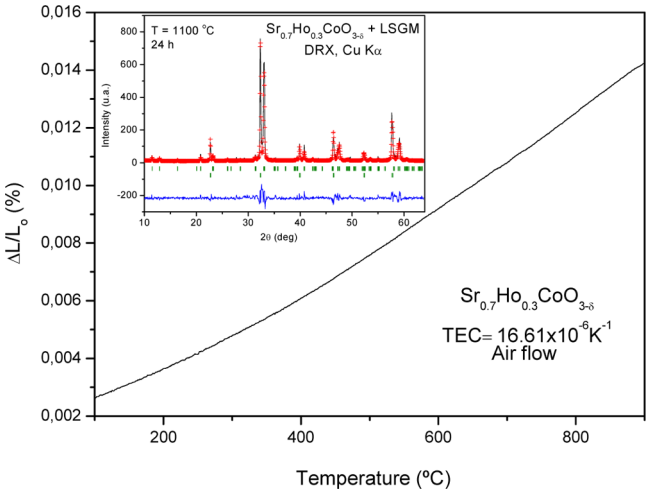

Figure 6. Thermal expansion determined by dilatometry of $Sr_{0.7}Ho_{0.3}CoO_{3-\delta}$. The inset shows the Rietveld-refined XRD profiles of a mixture of LSGM and $Sr_{0.7}Ho_{0.3}CoO_{3-\delta}$ after a thermal treatment at 1100 °C in air, showing no reaction products between both phases other than the initial reactants. The first and second series of Bragg positions correspond to $Sr_{0.7}Ho_{0.3}CoO_{3-\delta}$ and LSGM, respectively.

moderate thermal expansion and good compatibility with the electrolyte warrant the right accomplishment of the wanted tasks.

4. CONCLUSIONS

In summary, in this work a correlation between the excellent performances obtained in single cells[1] and the structural features obtained from NPD data has been established. The crystal structure has been refined from 25 to 800 °C in the tetragonal *I*4/*mmm* space group. The presence of a large number of oxygen vacancies at the working temperature along with high displacement factors suggests high oxygen-ion mobility. The diffusion of O^{2-} ions can be visualized by difference Fourier synthesis from NPD data collected at 800 °C, observing a significant spreading of the nuclear density within the tetrahedral layers, involving not only the labile O4 oxygens but also the O3 atoms located at the equatorial tetrahedral planes, thus configuring a 2D pathway for oxygen diffusion. The extraordinary performance obtained of $Sr_{0.7}Ho_{0.3}CoO_{3-\delta}$ can be thus related to the excellent ionic and electronic transport properties. The thermal expansion coefficient of 16.61×10^{-6} K^{-1} is somewhat higher than the values of the rest of the components of the SOFC; an excellent chemical compatibility with the electrolyte LSGM during 24 h is also observed.

AUTHOR INFORMATION

Corresponding Author

*Tel.: +34 91 334 9000. Fax: +34 91 372 0623. E-mail: vcascos@icmm.csic.es.

Notes

The authors declare no competing financial interest.

ACKNOWLEDGMENTS

We thank the financial support of the Spanish Ministry of Education to the project MAT2013-41099-R, and we are grateful to the Institut Laue-Langevin (ILL) for making all facilities available.

REFERENCES

(1) Liu, T.; Li, Y.; Goodenough, J. B. $Sr_{0.7}Ho_{0.3}CoO_{3-\delta}$ as a Potential Cathode Material for Intermediate-Temperature Solid Oxide Fuel Cells. *J. Power Sources* **2012**, *199*, 161−164.

(2) Tu, H. Y.; Takeda, Y.; Imanishi, N.; Yamamoto, O. $Ln_{0.4}Sr_{0.6}Co_{0.8}Fe_{0.2}O_{3-\delta}$ (Ln=La, Pr, Nd, Sm, Gd) for the Electrode in Solid Oxide Fuel Cells. *Solid State Ionics* **1999**, *117*, 277−281.

(3) Dokiya, M. SOFC System and Technology. *Solid State Ionics* **2002**, *152*, 383−392.

(4) Aguadero, A.; Faucett, L.; Taub, S.; Wolley, R.; Wu, K. T.; Xu, N.; Kilner, J. A.; Skinner, S. J. Materials Development for Intermediate-Temperature Solid Oxide Electrochemical Devices. *J. Mater. Sci.* **2012**, *47*, 3925−3948.

(5) Lei, Z.; Zhu, Q.; Zhao, L. J. Low Temperature Processing of Interlayer-Free $La_{0.6}Sr_{0.4}Co_{0.2}Fe_{0.8}O_{3-\delta}$ Cathodes for Intermediate Temperature Solid Oxide Fuel Cells. *J. Power Sources* **2006**, *161*, 1169−1175.

(6) Tsai, T.; Barnett, S. A. Effect of LSM-YSZ Cathode on Thin-Electrolyte Solid Oxide Fuel Cell Performance. *Solid State Ionics* **1997**, *93*, 207−217.

(7) Jiang, S. P.; Wang, W. Fabrication and Performance of GDC-Impregnated (La, Sr)MnO_3 Cathodes for Intermediate Temperature Solid Oxide Fuel Cells. *J. Electrochem. Soc.* **2005**, *152*, 1398−1408.

(8) Deng, Z. Q.; Yang, W. S.; Liu, W.; Chen, C. S. Relationship between Transport Properties and Phase Transformations in Mixed-Conducting Oxides. *J. Solid State Chem.* **2006**, *179*, 362−369.

(9) Tai, L. W.; Nasrallah, M. M.; Anderson, H. U.; Sparlin, D. M.; Sehlin, S. R. Structure and Electrical Properties of $La_{1-x}Sr_xCo_{1-y}Fe_yO_3$. Part 1. The System $La_{0.8}Sr_{0.2}Co_{1-y}Fe_yO_3$. *Solid State Ionics* **1995**, *76*, 259−271.

(10) Muñoz, A.; de la Calle, C.; Alonso, J. A.; Botta, P. B.; Pardo, V.; Baldomir, D.; Rivas, J. Crystallographic and Magnetic Structure of $SrCoO_{2.5}$ Brownmillerite: Neutron Study Coupled with Band-Structure Calculations. *Phys. Rev. B* **2008**, *78*, 054404.

(11) Takeda, Y.; Kanno, R.; Takada, T.; Yamamoto, O.; Takano, M.; Bando, Y. Phase Relation and Oxygen-Non-Stoichiometry of Perovskite-like Compound $SrCoO_x$ ($2.29 < x > 2.80$). *Z. Anorg. Allg. Chem.* **1986**, *540*, 259−270.

(12) Nagai, T.; Ito, W.; Sakon, T. R. Relationship between Cation Substitution and Stability of Perovskite Structure in $SrCoO_{3-\delta}$-based Mixed Conductors. *Solid State Ionics* **2007**, *177*, 3433−3444.

(13) Deng, Z. Q.; Liu, W.; Chen, C. S.; Lu, H.; Yang, W.S. Germanium and Iron Co-Substituted $SrCoO_{2.5+\delta}$ as Oxygen Permeable Membrane. *Solid State Ionics* **2004**, *170*, 187−190.

(14) Zeng, P.; Ran, R.; Chen, Z.; Zhou, W.; Gu, H.; Shao, Z.; Liu, S. Efficient Stabilization of Cubic Perovskite $SrCoO_{3-\delta}$ by B-site Low Concentration Scandium Doping Combined with Sol−Gel Synthesis. *J. Alloys Compd.* **2008**, *455*, 465−470.

(15) Li, Y.; Kim, Y. N.; Cheng, J.; Alonso, J. A.; Hu, Z.; Chin, Y.; Takami, T.; Fernández-Díaz, M. T.; Lin, H. J.; Chen, C. T.; Tjeng, L. H.; Manthiram, A.; Goodenough, J. B. Oxygen-Deficient Perovskite $Sr_{0.7}Y_{0.3}CoO_{2.65-\delta}$ as a Cathode for Intermediate-Temperature Solid Oxide Fuel Cells. *Chem. Mater.* **2011**, *23*, 5037−5044.

(16) Rietveld, H. M. A Profile Refinement Method for Nuclear and Magnetic Structures. *J. Appl. Crystallogr.* **1969**, *2*, 65−71.

(17) Rodríguez-Carvajal, J. Recent Advances in Magnetic Structure Determination by Neutron Powder Diffraction. *Phys. B* **1993**, *192*, 55−69.

(18) Istomin, S. Y.; Grins, J.; Svensson, G.; Drozhzhin, O. A.; Kozhevnikov, V. L.; Antipov, E. V.; Attfield, J. P. Crystal Structure of the Novel Complex Cobalt Oxide $Sr_{0.7}Y_{0.3}Co\ O_{2.62}$. *Chem. Mater.* **2003**, *15*, 4012−4020.

(19) Troyanchuk, I. O.; Karpinskii, D. V.; Sazonov, A. P.; Sikolenko, V.; Efimov, V.; Senyshyn, A. Effect of Iron Doping on Magnetic Properties of $Sr_{0.78}Y_{0.22}Co\ O_{2.625+\delta}$ - Layered Perovskite. *J. Mater. Sci.* **2009**, *44*, 5900−5908.

(20) Golosova, N. O.; Kozlenko, D. P.; Dubrovinsky, L. S.; Drozhzhin, O. A.; Istomin, S. Y.; Savenko, B. N. Spin State and Magnetic

Transformations in $Sr_{0.7}Y_{0.3}CoO_{2.62}$ at High Pressures. *Phys. Rev. B* **2009**, *79*, 104431.
(21) Withers, R. L.; James, M.; Goossens, D. J. Atomic Ordering in the Doped Rare Earth Cobaltates $Ln_{0.33}Sr_{0.67}CoO_{3-\delta}$ (Ln = Y(3+), Ho(3+) and Dy(3+)). *J. Solid State Chem.* **2003**, *174*, 198−208.
(22) Shao, Z. P.; Haile, S. M. A High-Performance Cathode for the Next Generation of Solid-Oxide Fuel Cells. *Nature* **2004**, *431*, 170−173.
(23) Svarcova, S.; Wiik, K.; Tolchard, J.; Bouwmeester, H. J. M.; Grande, T. Structural Instability of Cubic Perovskite $Ba_xSr_{1-x}Co_{1-y}Fe_yO_{3-\delta}$. *Solid State Ionics* **2008**, *178*, 1787−1791.